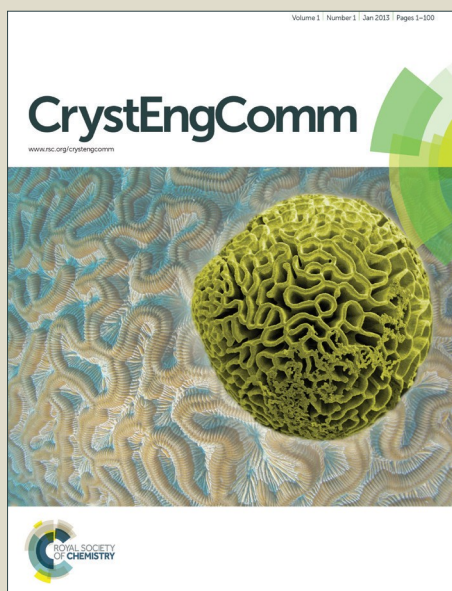


CrystEngComm

Accepted Manuscript



This article can be cited before page numbers have been issued, to do this please use: M. Cheng, X. Liu, Q. Luo, X. Duan and C. Pei, *CrystEngComm*, 2016, DOI: 10.1039/C6CE01455K.



This is an *Accepted Manuscript*, which has been through the Royal Society of Chemistry peer review process and has been accepted for publication.

Accepted Manuscripts are published online shortly after acceptance, before technical editing, formatting and proof reading. Using this free service, authors can make their results available to the community, in citable form, before we publish the edited article. We will replace this *Accepted Manuscript* with the edited and formatted *Advance Article* as soon as it is available.

You can find more information about *Accepted Manuscripts* in the [Information for Authors](#).

Please note that technical editing may introduce minor changes to the text and/or graphics, which may alter content. The journal's standard [Terms & Conditions](#) and the [Ethical guidelines](#) still apply. In no event shall the Royal Society of Chemistry be held responsible for any errors or omissions in this *Accepted Manuscript* or any consequences arising from the use of any information it contains.



Cocrystals of ammonium perchlorate with a series of crown ethers: preparation, structures, and properties

Minmin Cheng, Xun Liu, Qingping Luo, Xiaohui Duan*, Chonghua Pei

Received 00th January 20xx,
Accepted 00th January 20xx

DOI: 10.1039/x0xx00000x

www.rsc.org/

The three cocrystals of ammonium perchlorate (AP) with a series of crown ethers have been prepared successfully through solvent/antisolvent method, including 18-crown-6 (18C6), benzo-18-crown-6 (B18C6), and dibenzo-18-crown-6 (DB18C6). Crystal structures of three cocrystals characterized by single crystal X-ray diffraction (SXRD) reveal that all the cocrystals belong to the monoclinic system, in which the space group of 1:1 cocrystal of AP/18C6 and AP/B18C6 is $P2_1/n$, $P2_1/c$ for 1:1.5 cocrystal of AP/DB18C6. The main intermolecular interactions in three cocrystals are hydrogen bonds and π - π stacking. Powder X-ray Diffraction (PXRD) analyses have been performed to scrutinize the purity of the all crystals. The water contact angles of the three cocrystals were measured to be 0° (AP), 23.3° (AP/18C6), 25.4° (AP/B18C6), and 75.4° (AP/DB18C6), increasing with the number of phenyl group connected with crown ether, and the surface energy of three cocrystals are greatly decreased compared to AP. The thermal properties of the cocrystals were investigated by thermogravimetry-differential scanning calorimetry (TG-DSC) and hot-stage optical microscopy (HSOM). The results indicate that the decomposition peak temperatures of three cocrystals are greatly decrease compared to that of pure AP. Especially, the heat release increases from 475.5 J g^{-1} of AP to 1304.2 J g^{-1} for AP/B18C6 and 1488.4 J g^{-1} for AP/DB18C6. So, through delicately choosing the co-former of AP, cocrystallization can comprehensively tune the hygroscopicity and the thermal decomposition property of AP.

1. Introduction

AP has been widely employed as an oxidizer in composite solid propellants for rocket propulsion with its content in 60%-80% wt.¹⁻³ AP is known as a hardly replaceable oxidizer agent in rocket fuel because it is cheap and contains a large amount of oxygen that, in combustion, is entirely converted into stable gaseous reaction products.⁴⁻⁶

The thermal decomposition characteristics of AP influence the combustion behavior of the solid propellant directly, especially on the combustion. As is well known, decreasing temperature of the high-temperature decomposition (HTD) and increasing decomposition heat put a great on the performance of propellants.⁷ The lower the HTD temperature is, the shorter is the propellant ignition delay time, and the higher is the burning rate.⁸ Generally, a variety of catalysts have been applied to improve thermal decomposition behavior of AP, such as transition metal oxides.^{7,9,10} Besides, AP suffers from a

significant drawback, namely, the inherent hygroscopicity under ambient condition, which makes AP crystal easy to cake seriously, affect its normal storage, dispersity, fluidity, combustibility.^{1,3} To address the hygroscopicity problem, surface coating technology have been employed.¹¹ However, these two methods have not completely reaching the desired properties of AP. Especially, coating technology suffers the following unsatisfactory issues, such as, the flaking off of coating layer from AP, poor compatibility of coating materials with other components in composite solid propellants, energy loss if taking non-energetic coating materials. So, searching the novel methods to tune comprehensively the properties of AP is clearly of great urgency but a tremendous challenge.

Recently, improving the properties of explosives through cocrystallization has drawn intense research activity. Cocrystallization, as a complimentary technology,^{12,13} is suitable for generating superior materials to correct low density, high sensitivity,^{14,15} or low stability,^{15,16} which offers an effective method to regulate the properties of existing energetic materials at molecular level without changing their chemical structure. Therefore, in this work, we intend to investigate the effects of cocrystal formation on the properties of AP and expect to provide a new approach to improve the thermal behaviors and hygroscopicity of AP.

State Key Laboratory Cultivation Base for Nonmetal Composites and Functional Materials, Southwest University of Science and Technology, Mianyang 621010, P. R. China. E-mail: duanxiaohui@swust.edu.cn

Electronic Supplementary Information (ESI) available: Crystallographic data for three cocrystals, are available from Cambridge Crystallographic Data Centre, with CCDC NO. 1448027 for AP/18C6 cocrystal, NO. 1448025 for AP/B18C6 cocrystal, and NO. 1448026 for AP/DB18C6. For ESI and crystallographic data in CIF See DOI: 10.1039/x0xx00000x

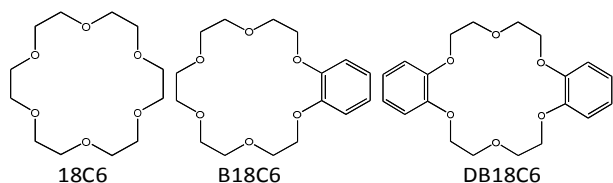


Fig. 1 Molecular structures of three crown ethers: 18C6, B18C6, DB18C6. Hydrogen atoms are omitted for clarity.

For the purpose of designing and reaching the desired properties, the choice for the co-former of cocrystal is of great importance. Usually, the cocrystal formation is based on the use of relatively strong intermolecular interactions, such as hydrogen or halogen bonds or strong π - π stacking.¹⁷⁻¹⁹ Crown ethers,²⁰ acting as the first generation of supramolecular hosts, have been extensively used in the areas of supramolecular chemistry and crystal engineering for variety of cationic species,²¹⁻²³ creating a variety of molecularly assembled architectures because of its multiple noncovalent interactions with complementary guest cations of the type DH_n^{m+} (NH_4^+ , H_3O^+ , RN_3^+ , etc.). The structure of the resulting supramolecular cationic species is controlled by the cavity size of the crown ether. Especially 18-crown-6 (18C6), one of a most simple relevant crown ether, is ideally suited.²⁸⁻³⁶ In term of a six-oxygen cavity size (cavity size 1.38 Å) and shape of 18C6, it can easily anchor NH_4^+ with the relative diameters of 1.48 Å.³⁷ The case is the same for the benzo-18-crown-6 (B18C6) and dibenzo-18-crown-6 (DB18C6), although the cavity size is reduced by the addition of phenyl ring which imparts rigidity to the crown moiety, the average cavity sizes for B18C6 and DB18C less than that of 18C6.³⁸ Making use of this recognition and self-assembly of crown ethers and ligands, the 1:1 cocrystal of ammonium nitrate (AN)-B18C6 was produced using the antisolvent precipitation method.³² Forming cocrystal not only could modify the morphology of AN, but also provide a means to minimize the drawbacks of polymorphic transition near ambient temperature, and caking and smoke generation upon burning caused by hygroscopic effect of AN. And cocrystallization experiments were carried out to study the efficacy of B18C6 as a cocrystallizing agent with urea, thiourea and their derivatives.³⁹

In this study, based on the recognition and self-assembly of the crown ethers to NH_4^+ ion through cavity size and non-bonding interactions, association of three different crown ethers to AP was investigated, including 18C6, B18C6 and DB18C6 (molecular structures see Fig. 1). The three crown ethers of interest were selected not only because of their similar cavity sizes and ion binding properties, but also the gradually increased hydrophobicity due to the introduction of phenyl group. It could be predicted that the hydrophobicity of the cocrystals of AP with the three crown ethers may increase with the phenyl group. Firstly, we prepared the cocrystals of AP with three crown ethers, 18C6, B18C6 and DB18C6, applying solvent/antisolvent method. Secondly, the generality of AP cocrystallization was scrutinized for three crown ethers, and the alteration of structures, wetting properties, thermal decomposition characteristics were elucidated.

2. Experimental

2.1 Materials

AP, 18C6 (99%), B18C6 (98%) and DB18C6 (>98%) were commercially available from Alfa Aesar China Chemical Co., Ltd, and methanol, N, N-dimethylformamide (DMF), and methyl tert-butyl ether (MTBE) with analytical grade from ChengDu Kelong Chemical Co., Ltd. Methanol and DMF were taken as solvent and MTBE as antisolvent. The chemicals and solvents were used without any further purification except AP.

2.2 Preparations of the cocrystals

AP/18C6 cocrystal: The cocrystal was prepared by solvent/antisolvent method. Equimolar amounts of AP (154 mg) and 18C6 (346 mg) were co-dissolved in 5ml methanol at 35°C, the solution was then slowly dropped into 50 ml MTBE by a pipette until the clear solution turned cloudy, and the mixed solution was kept for crystallization without further disturbances. Two hours later, the precipitated solid was filtered and the product was freeze-dried with a yield of 90%. Anal. Calcd. for $C_{24}H_{56}Cl_2N_2O_{20}$ (%): C, 37.74; H, 7.34; N, 3.70. Found: C, 38.05; H, 8.24; N, 3.46.

AP/B18C6 cocrystal: AP (137mg) and B18C6 (363mg) were co-dissolved in 8ml methanol at 35 °C, the solution was added into 80 ml MTBE drop by drop. Thereafter, the mixed solution was aged for 2 h under static conditions to crystallization. Then the cloudy solution was filtered and freeze-dried with a yield of 65%. Anal. Calcd. for $C_{16}H_{28}ClNO_{10}$ (%): C, 44.67; H, 6.52; N, 3.26. Found: C, 44.82; H, 6.58; N, 3.11.

AP/DB18C6 cocrystal: AP (123mg) and DB18C6 (377mg) were both dissolved in 4 ml DMF at 35 °C, the solution was then slowly dropped into 40 ml MTBE by a pipette under continuous stirring. The resulting solution was aged for 2 h under static conditions to crystallization. The white cocrystal was collected by filtration and freeze-drying with a yield of 74%. Anal. Calcd. for $C_{30}H_{40}ClNO_{13}$ (%): C, 54.70; H, 6.08; N, 2.13. Found: C, 54.60; H, 6.24; N, 1.72.

2.3 Characterization

Elemental Analysis. Elemental analysis was performed using a Vario-EL CUBE elemental analyzer for carbon, hydrogen, and nitrogen of the cocrystals.

Polarized optical microscopy. The colors caused by birefringence of all cocrystals and cocrystal habits were examined by an Olympus BX51-P microscope (Olympus, Tokyo, Japan) equipped with an U-AN360P polarizer, a DPIXEL 200 CCD camera, and a Motic Images Plus 2.0 ML digital camera software.

Single Crystal X-ray Diffraction. The single crystal X-ray diffraction (SXD) data of the cocrystals were collected with graphite-monochromated Mo-K α radiation ($\lambda = 0.071073$ nm) equipped with Gemini diffractometer in the temperature range 176-295K. Data collection was performed by Olex2 software package, and the structure was solved by full-matrix least-squares methods. The ShelXT and ShelXL programs were used for structure solution using Direct Methods and refinement respectively. All non-hydrogen atoms were refined

anisotropically and the hydrogen atoms were geometrically fixed.

Powder X-ray Diffraction. Powder X-ray Diffraction (PXRD) patterns were collected at room temperature (25 °C) using a PANalytical X'Pert PRO diffractometer operating at 40 kV and 40 mA with Cu K α radiation (1.54059 Å). Samples were scanned over the range of 3 to 60 degrees 2 θ at a scan rate of 0.4 degrees 2 θ /s. Calculated PXRD patterns were generated from the single-crystal structures of three cocrystals using Reflex in materials Studio 4.0 and compared with those obtained for the corresponding bulk samples.

Contact angle measurement. All sample powders were isostatically pressed into 1.5 mm-thick disks by a power press machine (FW-4A, China) with a pressure of 10 MPa, and the diameter of disks was 13 mm, the weight of disks was about 250 mg. The wetting properties of cocrystals were determined by contact angle measurements. The static contact angle measurement was performed with a KRÜSS Drop Shape Analyzer (Model DSA30, Germany) using the standard sessile drop method with Milli-Q water. A droplet of water was dropped on the disks at 20 °C. At least five droplets were applied onto sample disks and their contact angles were analyzed by fitting a tangent to the three-phase point where the liquid surface touched the solid surface.

Thermal Analysis.

Thermogravimetry-differential scanning calorimetry (TG-DSC).

The thermochemical behavior of the cocrystals were characterized by DSC and TG, which were recorded using United States SDT Q600 synchronous thermal analyzers in temperature range of 20–500 °C using aluminum crucibles with a single hole punched in the lids to allow to escape. The DSC-TG curves were conducted under nitrogen atmosphere of 100 mL min⁻¹ at a heating rate of 10 °C min⁻¹ and the average sample mass was about 2.0 mg (precision of 0.0001 mg).

Hot-stage Optical Microscopy (HSOM). Thermomicroscopic experiments were performed on Olympus BX51 microscope using a HCS601 Instec hot stage connected to a STC 200 temperature controller. The micrographs were recorded at 10 \times magnification using a camera being attached to the microscope. Contact thermal microscopy was conducted by heating start at room temperature using a 10 °C/min heating rate.

3. Results and Discussion

3.1 Structures of the Cocrystals

Table 1 Crystal data and structure refinement for three cocrystals

| Structural parameter | AP/18C6 cocrystal | AP/B18C6 cocrystal | AP/DB18C6 cocrystal |
|---|--|---|--|
| CCDC no. | 1448027 | 1448025 | 1448026 |
| Formula | C ₂₄ H ₅₆ Cl ₂ N ₂ O ₂₀ | C ₁₆ H ₂₈ ClNO ₁₀ | C ₃₀ H ₄₀ ClNO ₁₃ |
| Formula weight | 763.60 | 429.84 | 658.08 |
| Temperature/k | 176.41(10) | 292.36(10) | 294.39(10) |
| Crystal system | monoclinic | monoclinic | monoclinic |
| Space group | P2 ₁ /n | P2 ₁ /n | P2 ₁ /c |
| a/Å | 20.9447(9) | 14.2783(2) | 12.6348(2) |
| b/Å | 8.6823(3) | 9.93551(15) | 12.9180(2) |
| c/Å | 22.5551(11) | 14.7043(3) | 20.7752(3) |
| α /° | 90 | 90 | 90 |
| β /° | 118.257(6) | 99.5877(17) | 107.3603(17) |
| γ /° | 90 | 90 | 90 |
| Volume/Å ³ | 3785.3(3) | 2056.85(6) | 3236.38(9) |
| Z | 4 | 4 | 4 |
| D calc. (Mg/m ³) | 1.340 | 1.396 | 1.360 |
| μ /mm ⁻¹ | 2.230 | 2.155 | 1.639 |
| F (000) | 1632.0 | 911.0 | 1399.0 |
| Crystal size/mm ³ | 0.9 \times 0.4 \times 0.3 | 0.75 \times 0.25 \times 0.15 | 0.7 \times 0.6 \times 0.5 |
| Theta range for data collection/° | 7.746–134.146 | 9.456–134.092 | 10.034–134.102 |
| Index ranges | -26 $\leq h \leq$ 19, -10 $\leq k \leq$ 7, -25 $\leq l \leq$ 26 | -17 $\leq h \leq$ 16, -11 $\leq k \leq$ 7, -17 $\leq l \leq$ 13 | -14 $\leq h \leq$ 14, -10 $\leq k \leq$ 15, -24 $\leq l \leq$ 18 |
| Reflections collected | 20336 | 11060 | 19153 |
| Independent reflections | 6762 [R _{int} =0.0332] | 3671 [R _{int} =0.0313] | 5551 [R _{int} =0.0293] |
| Data/restraints/parameters | 6762/4/481 | 3671/4/277 | 5551/1/417 |
| Goodness-of-fit on F ² | 1.041 | 1.055 | 1.049 |
| R ₁ , wR ₂ (I > 2 σ (I)) | 0.0585, 0.1616 | 0.0706, 0.2059 | 0.0823, 0.2480 |
| R ₁ , wR ₂ (all data) | 0.0672, 0.1727 | 0.0774, 0.2167 | 0.0894, 0.2600 |



Fig. 2 Micrographs of the characteristic textures of the cocrystals by the polarized optical microscope: (a) AP/18C6, (b) AP/B18C6, and (c) AP/DB18C6 cocrystals

Table 2 Geometrical parameters for hydrogen bonds in AP/18C6 cocrystal

| N-H...O | N-H (Å) | H...O (Å) | N...O (Å) | ∠N-H...O (°) |
|--|---------|-----------|-----------|--------------|
| N _F -H _X ...O ₆ | 0.833 | 2.054 | 2.882 | 172.52 |
| N _F -H _C ...O ₄ | 0.835 | 2.006 | 2.822 | 165.28 |
| N _F -H _Y ...O ₅ | 0.798 | 2.108 | 2.904 | 175.40 |
| N _F -H _W ...O _L | 0.804 | 2.400 | 3.066 | 140.94 |
| N _G -H _A ...O _L | 0.877 | 2.193 | 3.096 | 155.10 |
| N _G -H _A ...O _H | 0.877 | 2.350 | 3.011 | 143.12 |
| N _G -H _Z ...O ₇ | 0.855 | 2.108 | 2.857 | 167.04 |
| N _G -H _B ...O ₈ | 0.732 | 2.128 | 2.853 | 170.81 |
| N _G -H _D ...O _E | 0.809 | 2.069 | 2.840 | 159.24 |

Symmetry operation: -x+1, -y+1, -z+1

Table 3 Geometrical parameters for hydrogen bonds in AP/B18C6 cocrystal

| N-H...O | N-H (Å) | H...O (Å) | N...O (Å) | ∠N-H...O (°) |
|--|---------|-----------|-----------|--------------|
| N ₆ -H _A ...O _A | 0.958 | 2.391 | 2.974 | 118.73 |
| N ₆ -H _A ...O ₄ | 0.958 | 2.025 | 2.926 | 155.50 |
| N ₆ -H...O ₂ | 0.947 | 2.290 | 2.861 | 118.03 |
| N ₆ -H...O ₃ | 0.947 | 1.949 | 2.870 | 163.29 |
| N ₆ -H _B ...O ₅ | 0.841 | 2.328 | 2.977 | 134.18 |
| N ₆ -H _B ...O ₇ | 0.841 | 2.128 | 2.837 | 141.55 |
| N ₆ -H _Y ...O ₈ | 0.956 | 2.032 | 2.989 | 176.85 |

Symmetry operation: x, y, z

The polarized optical microscopy images of three cocrystals are shown in Fig. 2. It can be seen that they all present rod-like morphology. The crystal structures were determined by single crystal X-ray diffraction and the crystallographic data are shown in Table 1.

AP/18C6 cocrystal produced from system of methanol-MTBE belongs to monoclinic system in the space group of P2₁/n with Z=4. The unit cell contains eight AP and eight 18C6 molecules, as shown in Fig. 3(a), and the NH₄⁺ joins with 18C6 to form a rotator-stator assembly. In AP/18C6 cocrystal, the N atom of NH₄⁺ is in the perching position, 0.894 Å out of the best plane of the oxygen atoms of the crown ring, which is the same as that reported in pervious literature.³¹ By analyzing the structure, it is found that molecule recognition and self-assembly of AP and 18C6 involve N-H...O hydrogen bonds. Possible hydrogen bonds have been marked with green dashed line in Figure 3(b) and the lengths and angles of the hydrogen bonds are listed in Table 2. The observed distances are all in the region for hydrogen bonds of this type.^{40, 41} It is hydrogen bond interactions and the size recognition between AP and 18C6 molecules that result in the formation of the AP/18C6 cocrystal.

The crystallographic parameters for AP/B18C6 cocrystal are also shown in Table 1. It reveals that AP and B18C6 molecules cocrystallize in a monoclinic system with space group P2₁/n and Z=4. The B18C6 possesses the C_{3v} coordination⁴² with guest molecule NH₄⁺, through hydrogen-bonding of N-H...O involving N(6)-H(A)...O(A), N(6)-H(A)...O(4), N(6)-H(A)...O(2), N(6)-H(A)...O(3), N(6)-H(B)...O(5), and N(6)-H(A)...O(7), as shown in Fig. 4(a). The ClO₄⁻ is bridged to NH₄⁺ as well as by hydrogen-bonding interaction of N(6)-H(Y)...O(8). All the hydrogen bonds have been marked with blue dashed line in Figure 4(a) and the lengths and angles of the hydrogen bonds are listed in Table 3. By analyzing the cocrystal structure, it is found that AP/B18C6 cocrystal molecules are stacked with significant π-π stacking interactions (see Fig. 4b), and the distances between molecular layers are 3.940 Å, with the ClO₄⁻ located in the upper left and lower right positions. The parallel molecular layers are connected into a network structure through N-H...O and π-π interactions.

Replacing the less symmetrical crown ether B18C6 with a more symmetrical DB18C6 has resulted in different mode of crystal packing in AP/DB18C6 cocrystal compared to the first two crystal structures. The AP/DB18C6 cocrystal produced from systems of DMF-MTBE belongs to monoclinic system in the

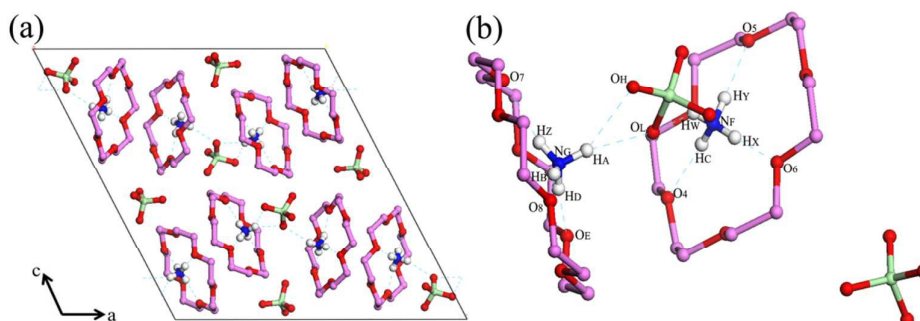


Fig. 3 (a) The unit cell of AP/18C6 cocrystal viewed along the *b*-axes. (b) The basic unit of AP/18C6 cocrystal. Possible hydrogen bonds are found in cocrystal, hydrogen atoms are omitted in 18C6 for clarity and hydrogen bonds are shown in blue dashed line. (atoms color as C in peak, H in white, O in red, N in blue, and Cl in green)

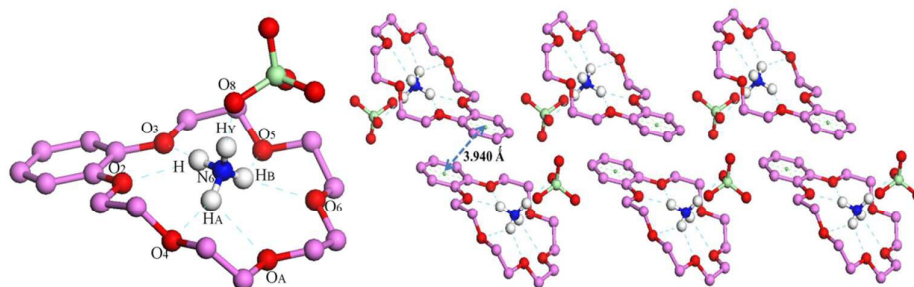


Fig. 4 (a) Basic unit of AP/DB18C6 cocrystal, and possible hydrogen bonds are found in cocrystal, hydrogen atoms are omitted for clarity and hydrogen bonds are shown in blue dashed line. (b) AP/DB18C6 cocrystal molecules stacked motif in columns parallel to the *b*-axis.

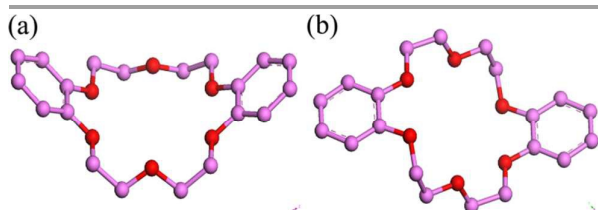


Fig. 5 Structure of DB18C6: (a) *cis*-DB18C6 and (b) *trans*-DB18C6. Hydrogen atoms have been omitted.

Table 4 Geometrical parameters for hydrogen bonds in AP/DB18C6 cocrystal

| N-H...O | N-H (Å) | H...O (Å) | N...O (Å) | ∠N-H...O (°) |
|--|------------|--------------|--------------|-----------------|
| N _B -H...O ₄ | 0.849 | 2.164 | 2.859 | 140.207 |
| N _B -H...O ₂ | 0.849 | 2.169 | 2.852 | 137.202 |
| N _B -H _C ...O ₆ | 0.844 | 2.184 | 2.877 | 139.127 |
| N _B -H _C ...O _A | 0.844 | 2.164 | 2.849 | 138.082 |
| N _B -H _{0AA} ...O ₅ | 0.849 | 2.260 | 2.902 | 132.453 |
| N _B -H _{0AA} ...O ₃ | 0.849 | 2.141 | 2.878 | 144.887 |
| N _B -H _B ...O ₁₇ | 0.820 | 2.225 | 3.003 | 158.181 |

Symmetry operation: *x, y, z*

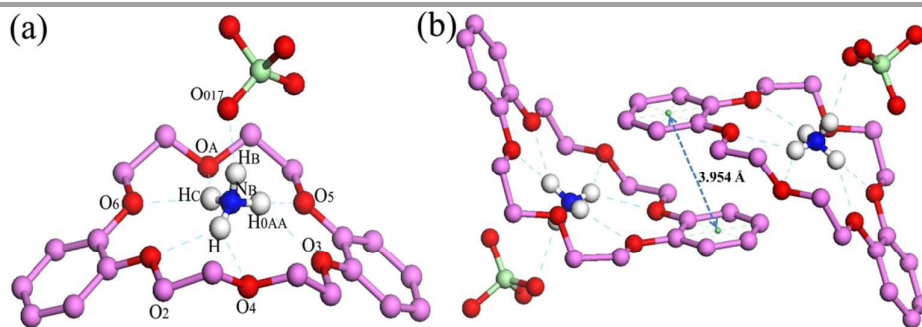


Fig. 6 (a) Basic unit of cocrystal of AP/DB18C6 and possible hydrogen bond found in cocrystal. Hydrogen atoms are omitted for clarity and hydrogen bonds are shown in dashed line. (b) π - π interaction between the two aromatic rings of two *cis*-DB18C6

space group of *P21/c* with $Z=4$. The cocrystal unit reveals 1:1.5 stoichiometry between the AP guest and DB18C6 host, in which DB18C6 exists two isomers-*cis* and *trans*. The molecule of *cis*-DB18C6 in structure has a butterfly conformation with approximate symmetry C_{2v} (see Fig. 5),^{43, 44} and the *trans*-DB18C6 is C_1 conformer, which the type of structure has been observed in other complexes of DB18C6 with the ammonium cation so far reported.⁴⁵ As shown in figure 6a, the AP/DB18C6 cocrystal structure is held together by the NH_4^+ with the *cis*-DB18C6 through hydrogen bonding and displays a rather unique host-guest relationship, in which three H atoms of NH_4^+ ions form hydrogen bonds with six O atoms of *cis*-DB18C6. The geometrical parameters for hydrogen bonds in AP/DB18C6 cocrystal are listed in Table 4. In addition, the main interactions between the two *cis*-DB18C6 are parallel-displaced π - π stacking between the two aromatic rings

(centroid...centroid distance 3.954 Å) as shown in Figure 6b. The AP/DB18C6 cocrystal molecules are infinite connected by all of these N-H...O hydrogen bonds and π - π stacking.

3.2 Power X-ray Diffraction Study

PXRD diffractogram provides another piece of information for the polymorphism and crystallinity of three cocrystals (Fig. 7). In particular, the calculated XRD diffractograms of the three cocrystals based on SXD show a close match with the experimental PXRD diffractograms. Similar diffraction patterns prove the bulk homogeneity and purity of the three crystalline solids.

3.3 Water contact angle and surface energies of cocrystals

The water contact angle has commonly been used as a criterion for the evaluation of hydrophobicity of a solid surface.

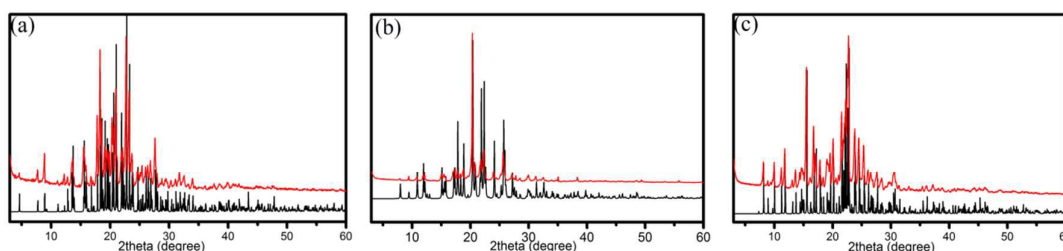


Fig. 7 Experimental diffractograms (red curves) and the calculated PXRD patterns based on SXD of cocrystals (black lines): (a) AP/18C6; (b) AP/B18C6; (c) AP/DB18C6 cocrystals.

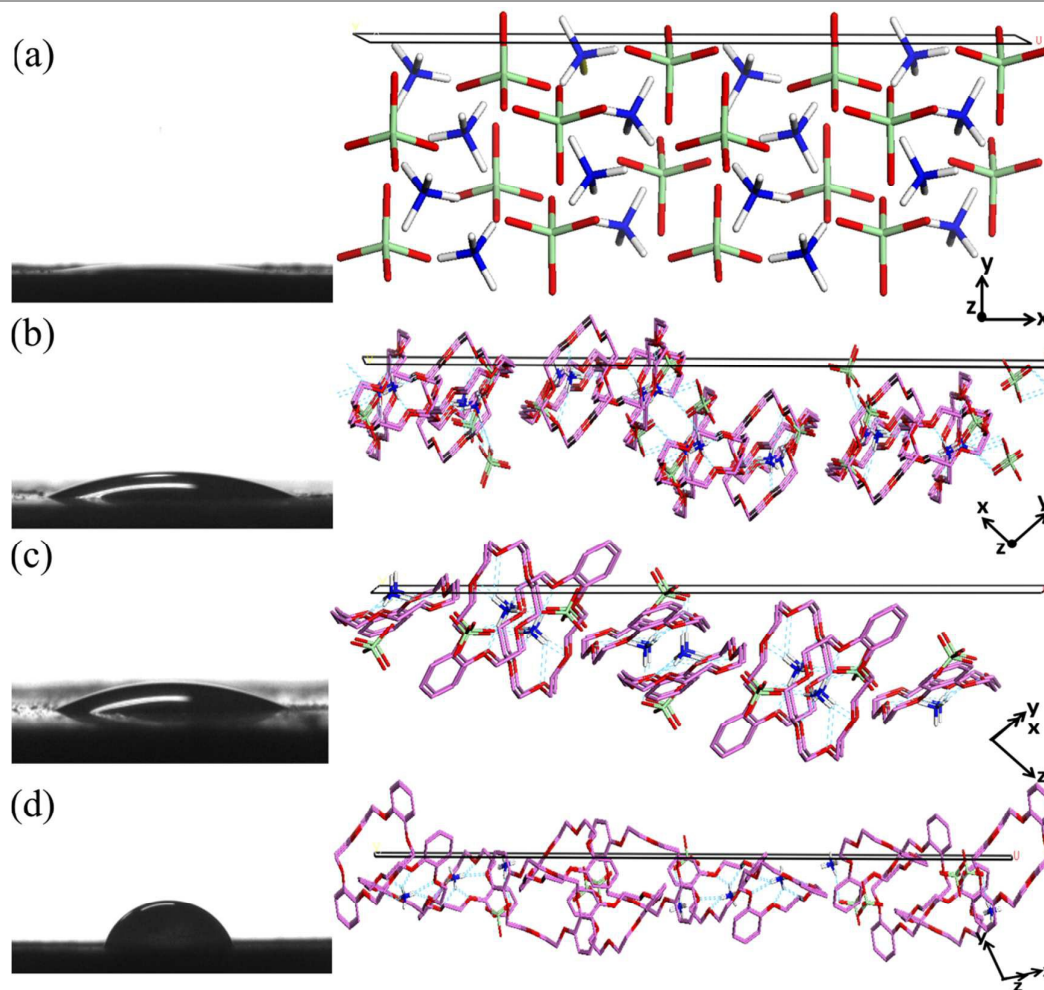


Fig. 8 Results of contact angle measurement using water droplets on the cocrystal disks and structure representation of the AP and three cocrystals along the (011) face, $(51\bar{2})$ face, $(21\bar{3})$ face and (131) faces, respectively. Hydrogen atoms are omitted for clarity and the structures correspond to the three-dimensionally periodic $2a \times 1b \times 2c$ supercells. [(a) AP, (b) AP/18C6, (c) AP/B18C6, and (d) AP/DB18C6]

The hydrophobicity characteristics of the cocrystals were investigated by using the sessile drop method. Figure 8 shows the images of the water droplets on the three cocrystal layers. The water contact angles of AP and three cocrystal layers are 0° , 23.3° , 25.4° , and 75.4° , respectively. As all we know, crown ether has hydrophobic outer skeleton, and there exist also hydrophobic phenyl groups in B18C6 and DB18C6, so, the contact angle increase of three cocrystals can be explained by

these hydrophobic groups. The surface chemistry and topography is crucial for understanding the hydrophobicity of a solid surface. As an example, we only display the structures of the AP⁴⁶ and three cocrystals along the (011), $(51\bar{2})$, $(21\bar{3})$ and (131) crystal faces (see Figure 8), respectively. And these crystal faces correspond to the strongest diffraction peak at $2\theta = 19.36^\circ$, 22.78° , 22.37° , 22.81° in the powder X-ray diffraction patterns. Examination of the face reveals a rather open and

rough surface topography on the molecular level. Due to the exposure of the hydrophobic outer skeletons and phenyl groups out of the surface, the water contact angles of three cocrystal layers have increased relative to that of pure AP. Of course, except the hydrophobic groups, the hydrophilic oxygen atoms of the crown ring and ClO_4^- ions are also observed at the crystal face of the three cocrystals. It is the difference of the densities and positions of the hydrophobic and hydrophilic groups at the surfaces that results in the different water contact angles, namely hygroscopicity.

In addition, the surface energy, which can directly tailor the hydrophobic behavior of surfaces, is another extremely important parameter. The surface energy (γ_{sv}^{TOT}), is the total surface and interfacial free energies existing at the solid-vapor boundary. According to the van Oss-Good theory, γ_{sv}^{TOT} involves both an apolar (γ_{sv}^{LW} , accounting for the Lifshitz-van der Waals type) component and polar (γ_{sv}^{AB} , accounting for Lewis acid-base interactions) component.⁴⁷

$$\gamma_{sv}^{\text{TOT}} = \gamma_{sv}^{\text{LW}} + \gamma_{sv}^{\text{AB}} \quad (1)$$

The modified contact-angle Young-Dupre equation becomes⁴⁷

$$\gamma_{LV}(1 + \cos\theta) = 2(\sqrt{\gamma_{sv}^{\text{LW}}\gamma_{LV}^{\text{LW}}} + \sqrt{\gamma_{sv}^{\text{AB}}\gamma_{LV}^{\text{AB}}} + \sqrt{\gamma_{sv}^{\text{LW}}\gamma_{LV}^{\text{AB}}}) \quad (2)$$

where θ is the contact angle at which a liquid-vapor interface meets the solid surface, the γ_{LV} is the surface energy of the liquid-vapor interface, and the γ^+ is the electron-acceptor (Lewis acid) and γ^- is the electron-donor (Lewis base) parameter. Three surface tension components (γ_{sv}^{LW} , γ_{sv}^{AB} , $\gamma_{sv}^{\text{LW}}\gamma_{sv}^{\text{AB}}$) can be determined by solving surface three simultaneous equations in the form of eq 2 using known surface tension components of two polar solvents and one apolar solvent, such as water, glycerol and paraffin oil.⁴⁸ The γ_{sv}^{AB} in eq 1 can be obtained from⁴⁷

$$\gamma_{sv}^{\text{AB}} = 2\sqrt{\gamma_{sv}^{\text{LW}}\gamma_{sv}^{\text{AB}}} \quad (3)$$

and the γ_{sv}^{TOT} was calculated from eq 1.

The surface free-energy component values of water, glycerol, and paraffin oil are reported in the literature⁴⁷. The contact angles, the surface free-energy components and surface energies of AP and three cocrystals are listed in Table 5 and 6,

respectively. As shown in Table 6, the surface energy of three cocrystal powders are less than that of AP.

Table 5 Contact Angle (°) of droplets of paraffin oil, glycerol, and water on the surfaces of AP and three cocrystals powder disks

| Powers | Paraffin oil | glycerol | water |
|-----------|--------------|----------|-------|
| AP | 0 | 0 | 0 |
| AP/18C6 | 2.7 | 46.7 | 23.3 |
| AP/B18C6 | 6.4 | 47.9 | 25.4 |
| AP/DB18C6 | 0 | 65.4 | 75.4 |

Table 6 Surface free-energy component values of AP and three cocrystals (MJ m^{-2})

| Powders | γ_{sv}^{LW} | γ_{sv}^{AB} | $\gamma_{sv}^{\text{LW}}\gamma_{sv}^{\text{AB}}$ | γ_{sv}^{TOT} |
|-----------|---------------------------|---------------------------|--|----------------------------|
| AP | 28.90 | 5.03 | 48.34 | 34.66 |
| AP/18C6 | 28.87 | 0.82 | 63.27 | 14.42 |
| AP/B18C6 | 28.72 | 0.75 | 62.37 | 13.83 |
| AP/DB18C6 | 28.9 | 1.13 | 8.95 | 6.36 |

Although the hygroscopicity of the three cocrystals does not reduce significantly compared to the pure AP, it provides a method to minimize the drawback of hygroscopicity, namely, delicately screening out the co-former to cocrystallize with AP, introducing hydrophobic groups in the chemical structure of co-former. Besides, it is also worth taking into account to shield the crystal faces with high-density of the hydrophilic groups by regulating the crystallization parameters or adding the additives in the crystallization process.

3.4 Thermal analysis

The DSC and TG thermograms of AP, crown ethers, and three cocrystals are shown in Figure 9 and Figure 10, and experimental data are listed in Table 7. In the DSC curves, the

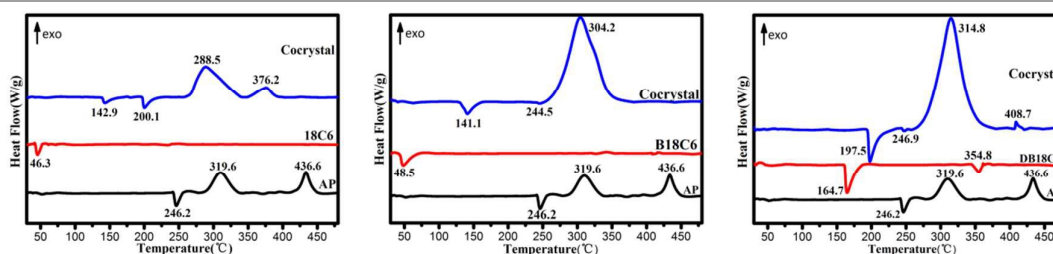


Fig. 9 DSC curves of AP, crown ethers and three cocrystals

thermal behaviors of the three cocrystals are completely different from AP. Three main thermal effects of AP are observed from DSC curve. Namely, the first endothermic peak at 246.2 °C is associated with a structure transition from orthorhombic to cubic phase,⁴⁹ and there are two obvious exothermic peaks centered at about 319.6 °C and 436.6 °C, which correspond to the low-temperature decomposition (LTD) and HTD, respectively. The heat of decomposition of pure AP is 475.5 $\text{J}\cdot\text{g}^{-1}$. For AP/18C6 cocrystal, it presents two endothermic

peaks (142.9 and 200.1 °C) and two exothermic peaks (288.5 and 376.2 °C), much lower than those of AP, and the apparent decomposition heat reading out from the DSC is 747.8 $\text{J}\cdot\text{g}^{-1}$. Surprisingly, different from the two exothermic peaks of AP and other two cocrystals, AP/B18C6 only presents one strong exothermic peak located at 304.2 °C. Meanwhile, the decomposition heat of AP/B18C6 increases from 475.5 $\text{J}\cdot\text{g}^{-1}$ of AP to 1304.2 $\text{J}\cdot\text{g}^{-1}$. The AP/DB18C6 cocrystal presents a very strong exothermic peak at 314.8 °C going with a negligible one

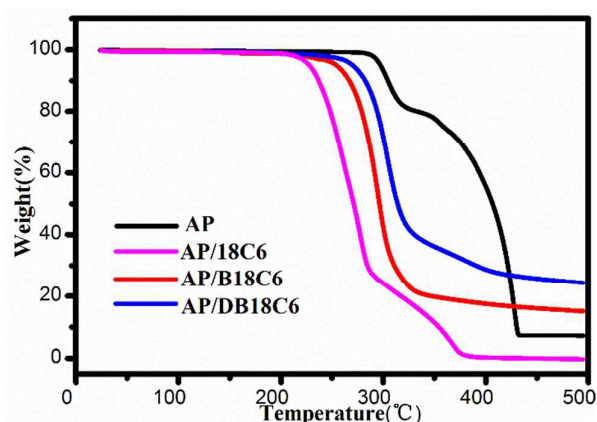


Fig. 10 TG curves of AP and three cococrystals

Table 7 Summarized results for DSC experiment of AP, crown ethers and three cococrystals

| Sample | Phase transition /°C | Melting point /°C | Endothermic decomposition/°C | Exothermic decomposition /°C |
|-----------|----------------------|-------------------|------------------------------|------------------------------|
| AP | 246.2 | - | - | 319.6 ; 436.6 |
| 18C6 | - | 46.3 | - | - |
| B18C6 | - | 48.5 | - | - |
| DB18C6 | - | 164.7 | 354.8 | - |
| AP/18C6 | 142.9 | 200.1 | - | 288.5 ; 376.2 |
| AP/B18C6 | - | 141.1 | 244.5 | 304.2 |
| AP/DB18C6 | - | 197.5 | 246.9 | 314.8 ; 408.7 |

at 408.7 °C, and this sharp and narrow exothermic peak at 314.8°C results in a high heat release of 1488.4 J·g⁻¹.

In addition, as shown in Figure 10, AP exhibits two weight loss steps. For the AP/18C6 cococrystal, two obvious weight losses occur in the temperature ranges of 211.3-294.2 °C and 301.4-392.7 °C, and the weight loss ratios respectively are 71.21%

and 29.40%. The obtained molar ratio 1:1 is consistent with that determined by the SXD analysis, illustrating thermal decomposition reactions of AP and 18C6 step by step. For the AP/B18C6 cococrystal, a rapid weight loss in one step appears from 250.8 °C to 329.0 °C and the weight loss ratio is up to be 82.13%. The AP/DB18C6 has two stages of weight losses, the first stage occurs from 259.8 to 317.9 °C with weight loss ratio of 60.50%, and the second stage from 327.4 to 412.0 °C with weight loss ratio of 15.00%. For these two cococrystals, the molar ratios from the TG are different from those by the SXD, showing the synergy effects of the thermal decomposition reactions of two components.

Furthermore, HSOM experiments led us to confirm and further elucidate the behavior of three cococrystals upon heating. The morphological changes and thermal events observed in the DSC experiments on three cococrystals were visualized under hot-stage microscope. The photomicrographs in Fig. 11 show the snapshots of the crystals at various temperatures. Melting of three cococrystals are observed at a higher temperature approximately range of 194-200 °C, 137-144°C, and 195-201 °C, respectively, which are consistent with the behavior observed in the DSC experiment. And the melting points of three cococrystals are higher than those of three crown ethers compounds. This phenomenon is in good agreement with previous report.⁵⁰ Further heating after their melting, AP/B18C6 and AP/DB18C6 cococrystals begin to be crushed into small crystals at 220 °C and 245 °C, and this observation may correspond to the endothermic decomposition temperatures on the DSC curves.

Thus, the DSC-TG results indicate that the thermal decomposition behavior of AP can be remarkably tuned by cococrystallization, especially AP/B18C6 and AP/DB18C6 cococrystals, showing better thermal properties, namely, lower HTD and higher heat release than those of AP.

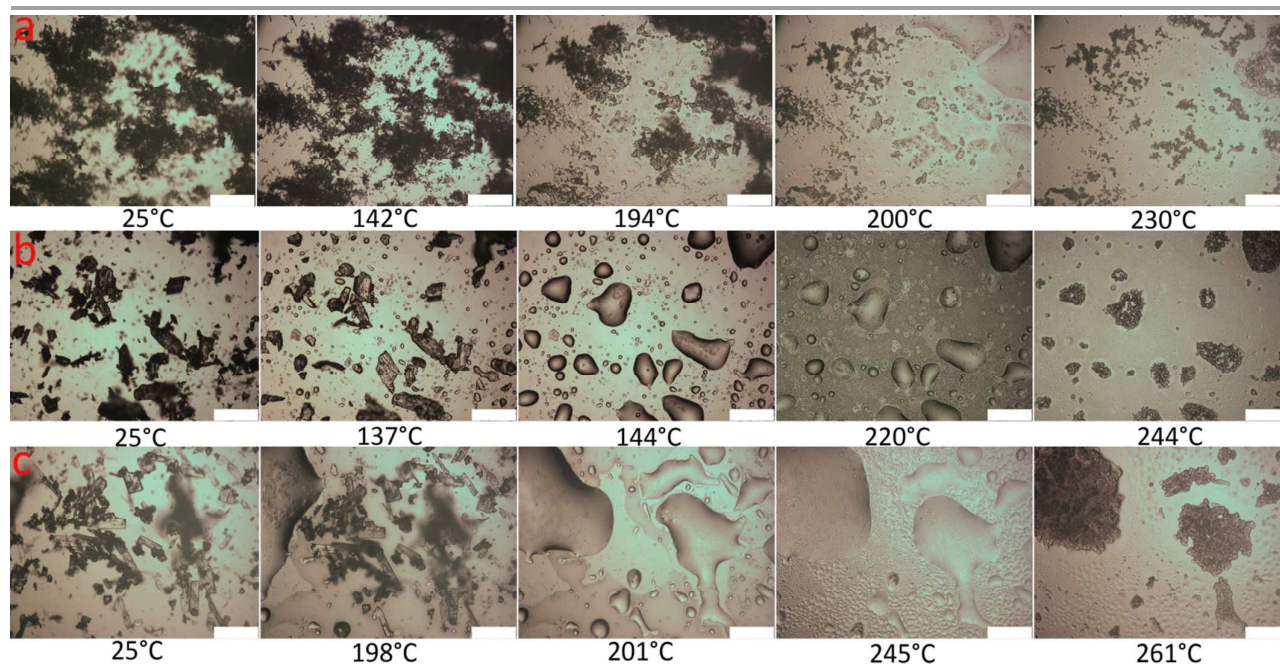


Fig. 11 Hot-stage optical micrographs at various temperatures [(a) AP/18C6, (b) AP/B18C6, and (c) AP/DB18C6 cocrystal]. The scale bar is 200 μm .

4. Conclusions

The AP/18C6, AP/B18C6 and AP/DB18C6 cocrystals were successfully prepared by a simple solvent/antisolvent method. The single crystal analysis was successfully applied to identify the new crystal structures. All the crystal structures depict supramolecular adduct formation between the hosts (crown ethers) and the guest (NH_4^+ ion) through cavity size and non-bonding interactions, namely, the hydrogen bonds and π - π stacking, and purity of the solids have been checked by PXRD analysis.

As has been shown in this study, the alterations in structure ultimately produce unique properties in the cocrystals. Based on the results of contact angles of AP and three cocrystals, 0° (AP), 23.3° (AP/18C6), 25.4° (AP/B18C6), and 75.4° (AP/DB18C6), it suggests that introducing hydrophobic groups in the chemical structure of the co-former is very important for the improvement of hygroscopicity of AP through cocrystallization technique.

The DSC curves of the three cocrystals display the unique thermal behaviors, completely different from the co-formers, especially AP/B18C6 and AP/DB18C6. Relative to two exothermic peaks of AP at 319.6°C and 436.6°C , AP/B18C6 cocrystal only shows a strong exothermic peak at 304.2°C . Meanwhile, the exothermic quantity of decomposition increases up to $1304.2\text{ J}\cdot\text{g}^{-1}$ from $475.5\text{ J}\cdot\text{g}^{-1}$ of AP. The AP/DB18C6 cocrystal presents a very strong exothermic peak at 314.8°C going with a negligible one at 408.7°C , and this strong peak at 314.8°C results in a high heat release of $1488.4\text{ J}\cdot\text{g}^{-1}$.

In a word, forming cocrystal provides a novel method to regulate simultaneously the hygroscopicity and thermal behaviors of AP through delicately screening out the co-former. As an oxidizer or propellant, the very important properties, such as burning rate, igniting ability, output flame temperature et al, will be discussed in our future work for these cocrystals.

Acknowledgements

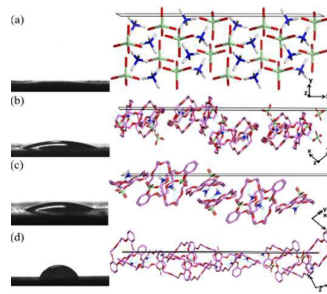
This work was financially supported by National Natural Science Foundation of China (No. 11572270), and the Postgraduate Innovation Fund Project by Southwest University of Science and Technology (No. 16ycx008).

References

- M. Yoo, S. Yoon and A. de Lozanne, *Journal of Vacuum Science & Technology B*, 1994, **12**, 1638-1641.
- G. d. Silva, S. C. Rufino and K. Iha, *Journal of Aerospace Technology & Management*, 2013, **5**, 139-144.
- A. L. Ramaswamy, H. Shin, R. W. Armstrong, C. H. Lee and J. Sharma, *Journal of Materials Science*, 1996, **31**, 6035-6042.
- S. J. Brzić, L. N. Jelisavac, J. R. Galović, D. M. Simić and J. L. Petković, *Hemijaska Industrija*, 2014, **68**, 435-443.

- T. Naya and M. Kohga, *Propellants, Explosives, Pyrotechnics*, 2013, **38**, 547-554.
- D. A. Reese, S. F. Son and L. J. Groven, *Propellants, Explosives, Pyrotechnics*, 2014, **39**, 684-688.
- G. Tang, S. Tian, Z. Zhou, Y. Wen, A. Pang, Y. Zhang, D. Zeng, H. Li, B. Shan and C. Xie, *The Journal of Physical Chemistry C*, 2014, **118**, 11833-11841.
- S. V. And and C. A. Wight, *Chemistry of Materials*, 1999, **11**, 3386-3393.
- H. Zhou, B. Lv, D. Wu and Y. Xu, *Materials Research Bulletin*, 2014, **60**, 492-497.
- S. Q. Tian, N. Li, D. W. Zeng, H. T. Li, G. Tang, A. M. Pang, C. S. Xie and X. J. Zhao, *Crystengcomm*, 2015, **17**, 8689-8696.
- W. U. Hao, L. I. Zhao-Qian and C. H. Pei, *Hanneng Cailiao/chinese Journal of Energetic Materials*, 2014, **22**, 482-486.
- Z. Yang, H. Li, H. Huang, X. Zhou, J. Li and F. Nie, *Propellants, Explosives, Pyrotechnics*, 2013, **38**, 495-501.
- N. Fischer, K. Karaghiosoff, T. Klapötke and J. Stierstorfer, *Zeitschrift Für Anorganische Chemie*, 2010, **636**, 735-749.
- T. M. Klapotke, F. A. Martin and J. Stierstorfer, *Angew Chem Int Ed Engl*, 2011, **50**, 4227-4229.
- M. H. Huynh, M. A. Hiskey, E. L. Hartline, D. P. Montoya and R. Gilardi, *Angew Chem Int Ed Engl*, 2004, **43**, 4924-4928.
- O. Bolton and A. J. Matzger, *Angew Chem Int Ed Engl*, 2011, **50**, 8960-8963.
- F. J. Hoeben, P. Jonkheijm, E. Meijer and A. P. Schenning, *Chemical Reviews*, 2005, **105**, 1491-1546.
- A. Gavezzotti, *Chemical Communications*, 2003, **27**, 309-314.
- P. Vishweshwar, J. A. McMahon, J. A. Bis and M. J. Zaworotko, *Journal of Pharmaceutical Sciences*, 2006, **95**, 499-516.
- C. J. Pedersen, *Science*, 1988, **241**, 536-540.
- M. Schaefer, *Angewandte Chemie International Edition*, 2003, **42**, 1896-1899.
- T. Chatterjee, M. Sarma and S. K. Das, *Crystal Growth & Design*, 2010, **10**, 3149-3163.
- S. Dong, Y. Luo, X. Yan, B. Zheng, X. Ding, Y. Yu, Z. Ma, Q. Zhao and F. Huang, *Angewandte Chemie*, 2011, **123**, 1945-1949.
- M. Bühl and G. Wipff, *Journal of the American Chemical Society*, 2002, **124**, 4473-4480.
- A. D. Bokare and A. Patnaik, *The Journal of Physical Chemistry A*, 2005, **109**, 1269-1271.
- S. J. Cantrill, D. A. Fulton, A. M. Heiss, A. R. Pease, J. F. Stoddart, A. J. White and D. J. Williams, *Chemistry—A European Journal*, 2000, **6**, 2274-2287.
- J. Kříž, J. Dybal, E. Makrlík and J. Budka, *The Journal of Physical Chemistry A*, 2008, **112**, 10236-10243.
- T. Mihelj, V. Tomasic, N. Biliskov and F. Liu, *Spectrochim Acta A Mol Biomol Spectrosc*, 2014, **124**, 12-20.
- Y. H. Luo, S. W. Ge, W. T. Song and B. W. Sun, *New J Chem*, 2014, **38**, 723-729.
- T. Chatterjee, M. Sarma and S. K. Das, *Crystal Growth & Design*, 2010, **10**, 3149-3163.
- K. N. Trueblood, C. B. Knobler, D. S. Lawrence and R. V. Stevens, *Journal of the American Chemical Society*, 1982, **104**, 1355-1362.
- T. Lee, J. W. Chen, H. L. Lee, T. Y. Lin, Y. C. Tsai, S. L. Cheng, S. W. Lee, J. C. Hu and L. T. Chen, *Chemical Engineering Journal*, 2013, **225**, 809-817.
- C. J. Pedersen, *J. Am. Chem. Soc.*, 1967, **89**, 7017-7036.
- P. Hurtado, F. Gamez, S. Hamad, B. Martinez-Haya, J. D. Steill and J. Oomens, *J Phys Chem A*, 2011, **115**, 7275-7282.
- J. Victor G. Young and A. G. Sykes, *Inorg. Chem.*, 1998, **37**, 376-378.

- 36 Z. Ge, J. Hu, F. Huang and S. Liu, *Angew Chem Int Ed Engl*, 2009, **48**, 1798-1802.
- 37 X. Tan, X. Duan, H. Li and C. Pei, *Micro & Nano Letters*, 2016.
- 38 A. Boda, S. M. Ali, M. R. Sheno, H. Rao and S. K. Ghosh, *Journal of molecular modeling*, 2011, **17**, 1091-1108.
- 39 S. Wishkerman, J. Bernstein and M. B. Hickey, *Crystal Growth & Design*, 2009, **9**, 3204-3210.
- 40 T. Steiner and G. R. Desiraju, *Chemical Communications*, 1998, **8**, 891-892.
- 41 G. R. Desiraju, *Accounts of Chemical Research*, 1996, **29**, 441-449.
- 42 P. Hurtado, F. Gámez, S. Hamad, B. Martínez-Haya, J. D. Steill and J. Oomens, *The Journal of Physical Chemistry A*, 2011, **115**, 7275-7282.
- 43 V. V. Yakshin, O. M. Vilkova, N. A. Tsarenko, S. V. Dyomin, V. I. Zhilov and A. Y. Tsivadze, *Doklady Chemistry*, 2005, **402**, 74-79.
- 44 V. V. Yakshin, O. M. Vilkova, N. A. Tsarenko and A. Y. Tsivadze, *Doklady Chemistry*, 2010, **430**, 32-34.
- 45 C. S. Choi, H. J. Prask and E. Prince, *Journal of Chemical Physics*, 1974, **61**, 3523-3529.
- 46 P. Dapporto, P. Paoli, I. Matijašić and L. Tušek-Božić, *Inorganica Chimica Acta*, 1996, **252**, 383-389.
- 47 M. Dogan, M. S. Eroglu and H. Y. Erbil, *Journal of Applied Polymer Science*, 1999, **74**, 2848-2855.
- 48 T. Lee and S. C. Chang, *Crystal Growth & Design*, 2009, **9**, 2674-2684.
- 49 V. V. Boldyrev, *Thermochimica Acta*, 2006, **443**, 1-36.
- 50 L. Bereczki, K. Marthi, P. Huszthy and G. Pokol, *Journal of Thermal Analysis & Calorimetry*, 2004, **78**, 449-459.



The thermal behaviors and hygroscopicity of AP have been simultaneously improved through cocrystallization with 18C6, B18C6, and DB18C6.